

Received February 20, 2015, accepted March 6, 2015, date of publication March 30, 2015, date of current version May 7, 2015.

Digital Object Identifier 10.1109/ACCESS.2015.2414815

# Open Source SDR Frontend and Measurements for 60-GHz Wireless Experimentation

PER ZETTERBERG<sup>1</sup> and RAMIN FARDI<sup>2</sup>

<sup>1</sup>Access Linnaeus Center, KTH Royal Institute of Technology, Stockholm SE-100 44, Sweden

<sup>2</sup>Bluewave Microsystems AB, Kista SE-164 05, Sweden

Corresponding author: P. Zetterberg (perz@kth.se)

This work was supported by Wireless@KTH through the Small Project call 13/02.

**ABSTRACT** This paper aims to make 60-GHz experimentation possible for a wider range of research groups.

We do this by describing a low-cost front-end that can be used in combination with any baseband processing platform. We provide detailed instructions and software for connection with the USRP N200/N210, including general classes for controlling the board and example single-input single-output and  $2 \times 2$  Multiple-Input Multiple Output applications. In addition, we provide measurements to assess the impact of phase noise and other hardware impairments in low-cost millimeter-wave systems for hybrid measurement and simulation studies. Finally, we also perform performance measurements on the hardware. All our materials, such as the hardware design, the software, and the measurements, are freely available.

**INDEX TERMS** Wireless.

## I. INTRODUCTION

Communication over increasingly higher carrier frequencies is a prevalent trend in wireless systems development [1]. This development has been enabled by advances in silicon chip technology in recent years [2]. The new carrier frequencies have different properties in terms of propagation parameters such as path-loss, fading, delay-spread and angle-spread than conventional lower frequency bands [3], [4]. In addition, higher levels of analog hardware impairments e.g. in the form of amplifier non-linearity, phase-noise, and IQ imbalance may be expected [5]. New deployment scenarios such as ultradense networks and massive Multiple-Input Multiple Output (MIMO) are also foreseen [6]–[8]. The use of wide communication bandwidths and narrow beamwidths make the scenario radically different from cellular networks at lower bands. The recent 60GHz standards IEEE 802.11ad and IEEE 802.15.3c provide means to use narrow-beams using e.g. antenna switching or phase-shifters, see [9] and [10], in order to significantly improve the link budget. Improved beamforming, feedback, and spatial multiplexing schemes for mm-wave systems is also an active research topic [11]–[13]. Early measurement results suggest multi-gigabit capacity and operation in both line of sight (LoS) and non-LoS see [1], [13], [14] is possible. Radio over fiber in the context of mm-wave is also getting attention [15].

Research groups who want to address mm-wave communications may use models for the various phenomena.

However, such studies should be complemented with the use of measurements and implementation studies. This makes it possible to verify the practical usefulness of the algorithms and systems, identify missing pieces in system design and to perform proof of concept demonstrations.

Since the mid-2000s, experimentation in wireless communication has been made affordable and accessible to university groups by commodity software defined radio platforms such as the USRP ([www.ettus.org](http://www.ettus.org)), WARP (<http://mangocomm.com/>) and others.

For experimentation with mm-wave, researchers can use the VubiQ development kit (<http://www.admiral-microwaves.co.uk/vubiq-development-systems.php>), which is used in [12]. It is also possible to use functional radio links such as the Wilocity chipset used in Dell 6430u laptops and HXI Gigalink 6451 radios (<http://www.hxi.com/datasheets.asp>), or Vizio XWH200 wireless HDMI TX-RX pairs, which are used in [14] and [16], respectively. The disadvantage of this approach is that the channel can only be indirectly observed through measurements of link statistics such as throughput and RSSI. Also, the approach does not allow much experimentation with new air interfaces and radio resource management schemes. Another option is to use up/down-converters, (see <http://www.siversima.com/products/millimeter-wave-converters/>), connected to e.g. a 2.4GHz platform.

However, as of now, there is no open-source simple solution for mm-wave experimentation. We are filling this

gap by introducing an open source radio front-end design which can be connected to a commodity software defined radio. The design is completely open. We provide Gerber files, drill files, schematics and software. Thanks to the built-in antenna on the 60GHz circuit used HMC6000LP711E and HMC6001LP711E, see [www.hittite.com](http://www.hittite.com), a simple two-layer FR4 substrate with low requirements can be used. A seemingly similar design is used in [17], but the paper provides little detail and focuses on example applications.

This paper also presents measurement results characterizing the performance in terms of transmitted EIRP, noise figure, third and fifth order inter-modulations and phase-noise. These measurements are useful for researchers as a reference, and to be able to estimate what can be expected by the platform in different scenarios.

In the paper, we also describe the structure of the software we have created, its application interface and how to build new applications using the interface. The software is made for the USRP N200/N210 boards, but can be transferred to any platform with access to general purpose output and input pins. Example applications for single-input single-output (SISO) and  $2 \times 2$  MIMO are presented. The companion video demonstrates  $2 \times 2$  MIMO operation with spatial multiplexing. To the best of our knowledge this is the first published demonstration of spatial multiplexing at 60GHz.

Measurement traces of phase-noise and  $2 \times 2$  MIMO signals are also presented. Phase-noise is generally modeled by Wiener processes or the Ornstein-Uhlenbeck process [18], [19]. However, using our measurements, actual phase-noise processes can be used in the simulations. Phase-noise compensation algorithms is a hot-topic in communications research [20], [21]. Our measurements are ideal for testing such algorithms since we use a low-cost high frequency application where such algorithms, are most beneficial.

The phase-noise traces focus on a single source of impairment only. In low-cost systems, there are also other signal impairments [5]. Overcoming and analyzing the effects of these impairments is the topic of dirty-RF [22]. We have also measured and made available  $2 \times 2$  MIMO signals that aim to capture all the impairments in our system. This is unlike traditional MIMO channel measurements which only characterize the linear response between the transmitters and receivers. The  $2 \times 2$  MIMO signals are captured in such a way that power control and detection schemes can be investigated offline using mild assumptions, thereby facilitating such research.

The paper is organized as follows. Section II describes the hardware while Section III discusses its beamsteering possibilities. Then in Section IV, all aspects of integration with a USRP N200/N210 are covered. Connection to other platforms is discussed in Section V. Performance parameters related to link budget non-linearities are presented in Section VI. Openly available measurements for hybrid simulations and measurement studies are

presented in Section VII, with phase-noise measurements in Section VII-A and  $2 \times 2$  MIMO measurements in Section VII-B. Section VIII describes the open materials accompanying in the paper. Finally Section IX concludes the paper.

## II. THE FRONT-END

The front-end is divided into three boards: TX, RX and CLK. This design makes it easy to configure multiple-boards in a MIMO setup (including massive MIMO). The boards can also be used separately in e.g. relaying experiments. The user can easily switch between different setups using a single set of boards. The solution also has some flexibility in terms of antenna placement. The following three sections describe each of the three boards. Hardware design files are available, see Section VIII. The boards are two-layer PCBs with a ground plane and a signal plane on a 1.6mm thick FR4 substrate with copper traces of  $18\mu\text{m}$  thickness.

### A. TX BOARD

The front end TX board is designed around the Hittite HMC6000LP711E chip. The chip contains a direct upconversion transmitter chain and an integrated antenna. The antenna is linearly polarized and has peak gain of 7.5dBi and a 10dB beamwidth of around 120 degrees. The antenna diagram is approximately  $\cos^2(\theta)$  shaped in both azimuth and elevation. The orientation of the polarization is indicated on the PCB board. The chip has balanced connections for base-band I and Q signals. A picture of our TX board is shown in Fig. 1. To make the board easily usable with standard signal generators as well as the USRP, we have mounted baluns between the HMC6000LP711E chip and the input I and Q MCX connectors. This provides an input with a normal  $50\ \Omega$  single ended MCX connector. The TX board also has two MCX connectors for the differential inputs of a 285.714MHz (or 308.570MHz) clock. By connecting the same clock to several boards - coherent beamforming and MIMO transmissions can be performed. The clock is generated and distributed by the CLK board, described in Section II-C below.

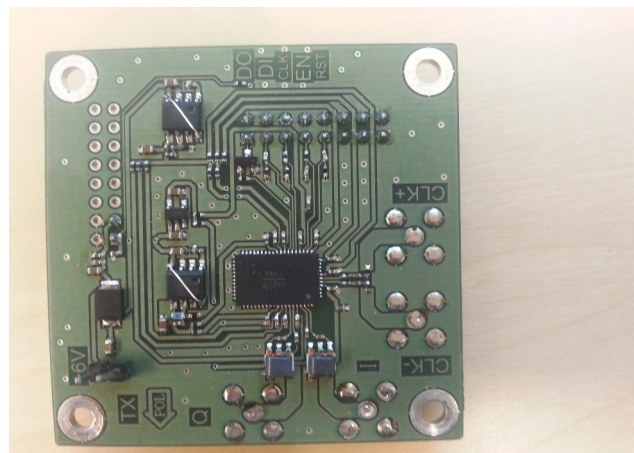


FIGURE 1. TX board.

The board has two sixteen-pin 2.54mm headers. One of them (JP1) is used for the digital control of the board. The other header is used for +6V supply voltage and a 3.3V input digital reference level. The digital connections are designed to interface with a 3.3Volt logic system, while the HMC6000LP711E chip itself uses 1.2Volt logics. There are four logic input signals: SEN, SDI, SCLK and SRST, and one output: SDO. The electrical connection of these signals can be found in the schematic for the board. The programming of the chip is described in its user manual, although many details are unclear. However, our code for the USRP see Section IV-B, provides a tested reference implementation that shows in detail how to control the chip. The gain control of the transmitter is obtained by varying the “IF attenuation” of the chip (see [http://hittite.com/content/documents/data\\_sheet/hmc6000lp711e.pdf](http://hittite.com/content/documents/data_sheet/hmc6000lp711e.pdf)). The highest gain setting is 13, which corresponds to a zero IF attenuation setting.

### B. RX BOARD

The RX front end board is based on the Hittite HMC6001LP711E chip. The antenna gain is 7.5dBi and the antenna diagram similar to the transmitter. The linear polarization direction is indicated on the PCB. The board has four MCX connectors (as has the RX board). Two of them are single-ended outputs corresponding to the I and Q part of the downconverted signal. The two remaining MCX connectors are for the balanced input from the CLK board. The digital and power connections are identical to the TX board. The board also has a two pin header, JP3 (as has the TX board), which can be used to distribute power to the clock board. The gain of the receiver is set by controlling the “IF attenuation” and “baseband attenuators” of the chip (see [http://hittite.com/content/documents/data\\_sheet/hmc6001lp711e.pdf](http://hittite.com/content/documents/data_sheet/hmc6001lp711e.pdf)). However, according to our measurements with the USRP N210, the base-band gain does not improve the SNR and thus we only control the IF attenuation. This choice also reduces the risk of saturating the USRP N210 analog-to-digital converter.

### C. CLK BOARD

The CLK board (clock board) is designed in a flexible way to allow an arbitrary number of RX and TX boards to run phase coherently. To facilitate this, the CLK board has two modes - master and slave. In the master mode, the clock signal is generated by the on-board crystal (Vectron VCC6-QCE-285M7140000 or Vectron VCC6-QCE-308M570000) and distributed on two balanced outputs CLK+/CLK-. Master and slave configurations are selected by changing the position of the strap position of header P1. In slave mode, the clock is obtained externally and fed to the board through the MCX connector CLK\_IN. Boards in both modes send a buffered version of the clock on CLK\_OUT.

Several CLK boards can be synchronized by the daisy chain principle. Clock boards always acting as slaves do not need to be populated with a crystal. A slave board can also

be fed with the signal from a regular signal generator, which can be useful for certain measurements. The signal generator should then produce a CW with frequency 285.714MHz or 308.570MHz, and an amplitude of 6dBm.

The choice of clock frequency (285.714MHz or 308.5714MHz) depends on the desired channel spacing. With a 285.714MHz clock, a 500MHz channel spacing is achieved while the 308.5714MHz yields a 540MHz channel spacing. Thus, in the former case the carrier frequencies are nominally 57GHz, 57.5GHz,...,64GHz while in the latter they are 57.24GHz, 57.78GHz,...,63.72MHz.

### III. BEAMSTEERING

Each TX and RX board has a 3dB beamwidth of around 90-degrees in both azimuth and elevation. Multiple boards can thus be used to cover different parts of the complete sphere. To obtain narrower sectors multiple boards need to be combined. As mentioned above, the TX and RX boards presented in this paper can be phase-locked by chaining CLK boards. This forces the phases of multiple boards to be coherent, as will be verified by the “long-term phase stability” measurements in Section VII-A. However, the phase of each board is random at startup, and thus a transmitter array would need an auxiliary RX board to calibrate the phase of each transmitter (and vice versa for a receiver array). Another limitation is the size of the board, which is 55mm or 11 wavelengths. An array created with these inter-element distances will have many sidelobes of comparable strength to the main lobe. However, the array gain achieved will still be the same, e.g. 10 elements will still yield 10dB just as in a closely spaced array. To reduce the sidelobes, the RX and TX boards could be re-designed with multiple HMC6000LP711E and HMC6001LP711E chips per board. Since the size of the chips are  $7 \times 11\text{mm}$ , a one dimensional linear array would therefore have a minimum spacing of 1.4 wavelengths, which would still provide a few significant sidelobes. However, the sidelobe level could be reduced by arranging the chips in an irregular fashion [23].

There exists a version of the Hittite chipset with external antenna connector (called HMC6000 and HMC6001). These can be connected to an external antenna although it would be an elaborate and difficult process [24], [25]. These chips are small enough to allow 0.5 wavelength spacing in one dimensional arrays.

### IV. CONNECTION TO USRP

#### A. HARDWARE

The front-end can be connected to a USRP N210s equipped with BasicRX and BasicTX boards ([www.ettus.com](http://www.ettus.com)). Connections to other USRP models should be straightforward. The use of the BasicTX and BasicRX boards eases both the hardware and software interface to the USRP. It also simplifies the use of the board, together with other base-band sources and sinks. In addition, it makes it possible to arrange the positions of the antennas independently of the position of the USRP.

The digital control and voltage connections are obtained by connecting a ribbon between the J50 and J46 connectors of the BasicTX board and the JP1 and JP2 headers of the TX board (the headers are 2.54mm 2 × 8), see Fig. 2. The J50 connector allows the use of the io\_tx [0] to io\_tx [7] signals of the USRP to be used to control the board.

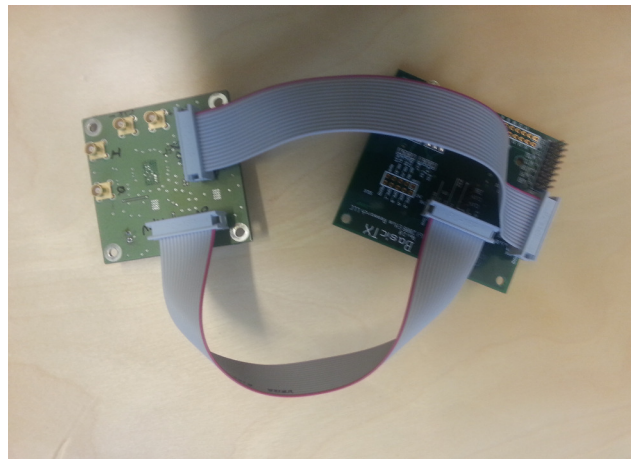


**FIGURE 2.** Digital connections between BasicTX and TX board.

With minor modifications of the software we provide, it is possible to connect a second TX board to the digital controls of header J51 on the BasicTX board and thereby control two boards from one USRP.

The TX-A and TX-B SMA connectors of the BasicTX board are used as base-band I & Q signals. We have chosen the center frequency 70MHz for the based-band signals. Thus, we set the RF frequency to 70e6 when operating the USRP via the UHD driver. The UHD driver is developed by Ettus Research ([www.ettus.com](http://www.ettus.com)) to interface PC software with their line of USRPs and daughterboards. Since the UHD driver is unaware of our external 60GHz hardware, 70MHz is the RF frequency from its point of view, since it is the output frequency of the BasicTX board. In order to filter out overtones and image frequencies, a SBP-70 filter from mini-circuits ([minicircuits.com](http://minicircuits.com)) is placed between the TX-A SMA connector of the BasicTX and the MCX Q connector of the TX board and another SB-70 filter between TX-B and MCX I connectors. Naturally, two MCX-SMA cables and two SMA-SMA cables are needed. Care must be taken so that the cables have equal lengths.

The RX board is connected in the same way as the transmitter. Ribbon cables are fitted between the J24 and J16 connectors of the BasicRX board and JP1 and JP2 headers of the RX board. As in the transmitter SBP-70 filters are used between the I and Q MCX output signals and RX-A and RX-B connectors of the BasicRX board.

We have created an example OFDM modulation for use with the 60GHz front-end boards (see Section IV-B below). This modulation can be used with a host sample-rate of 25Msps or 50Msps. The RF bandwidth of the transmitted signal is then less 22MHz, which fits well with the

SBP-70 filter. When using the OFDM modulation, an RMS value of 5000 is suitable for the samples sent to the UHD driver through the command `uhd::tx_streamer::send` (we are here using the `complex<int16>` host format representation). The base-band signal centered at 70MHz then has a power of around  $-20\text{dBm}$ .

### B. SOFTWARE

In order to control the RX and TX boards from the USRP, three C++ classes has been defined: `board_60GHz_base`, `board_60GHz_TX` and `board_60GHz_RX`. The base class contains the functionality necessary to read and write to the registers of the RX or TX chip, while the specifics are defined in the separate TX and RX classes. When the TX and RX boards are instantiated, the boards are set to the default carrier frequency, 60GHz, and maximum gains. The methods `set_gain` and `set_freq` of the respective method are used to change these parameters, which can be done on the fly.

The use of the TX and RX class is illustrated by the example programs `tx_60GHz.cpp` and `rx_60GHz.cpp`, respectively. These are similar to the example programs `tx_samples_from_file.cpp` and `rx_samples_from_file.cpp` which are provided as open source by Ettus Research distributed with their UHD driver package.

To further support users, two Matlab/Octave functions `tx_60GHz.m` and `rx_60GHz.m` have been created. These functions call the corresponding C++ programs, and thereby provide an interface to transmit and receive using the boards. Functions in C++ and Matlab/Octave have also been created for use with a  $2 \times 2$  MIMO setup where the transmitting and receiving pair of USRP N210 are synchronized using a Ettus Research MIMO cable.

In the receiving programs, the maximum sample rate for sixteen bit over-the-wire (OTW) transfers is 25Msps, while 50Msps can be achieved with eight bit OTW transfers. In the latter case, the user need to know beforehand the maximum amplitude at the receiver. This is all standard USRP N210 use. However, we have introduced a new feature for 8-bits 50Msps OTW transfer where the maximum amplitude is automatically set at the receiver. This is based on preliminary reception of 363 samples of the signal with 16-bits OTW format and 50Msps rate prior to the actual capture of data (this is possible due to the short duration of 50Msps sampling).

A pair of Matlab/Octave scripts for running a simple OFDM modulation over the 60GHz hardware is given in the scripts `demo_tx.m` and `demo_rx.m`. An example constellation scatter plot obtained in the receiver using these scripts is shown in Fig. 3. A  $2 \times 2$  MIMO version with spatial multiplexing of two modulation streams which is given by the corresponding scripts `demo_MIMO_tx.m` and `demo_MIMO_rx.m`.

The modulation format is in both cases OFDM with a DFT size of 40, of which 17 subcarriers are used and the remaining 23 nulled. With a sampling frequency

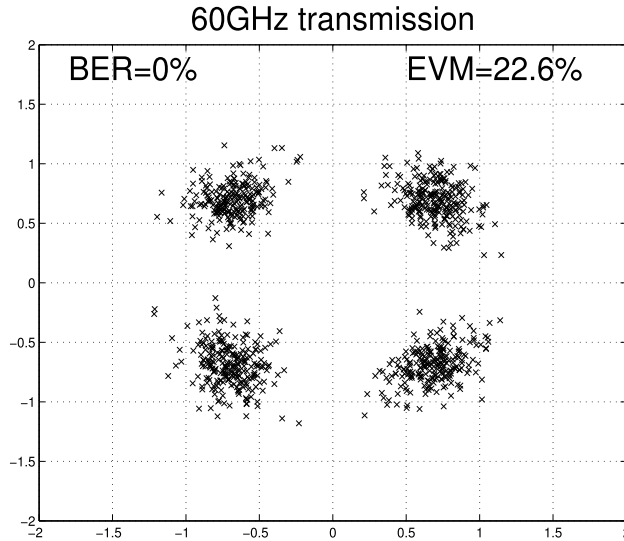


**FIGURE 3.** Scatter plot from the SISO OFDM example code.

of 25Msps, this corresponds to a subcarrier spacing of 625kHz. One subcarrier is used for common phase error correction in the SISO case, and two in the  $2 \times 2$  MIMO case (one per transmit antenna). Two full OFDM symbols are used for channel estimation in the SISO case and four in the  $2 \times 2$  MIMO case (two per transmit antenna). The modulator and demodulator are implemented in the Matlab functions `modem_OFDM4.m` and `demod_OFDM4.m`, respectively. A synchronization sequence is added to the beginning of the transmitted frames, which is used for timing and frequency-offset estimation at the receiver using the function `synchronize_OFDM1.m`. The operation of the system is demonstrated in the companion video.

These demo scripts have a parameter `use_50Msps`, which can be used to select the higher sampling frequency. The performance is limited by the linearity in both the 25Msps and 50Msps case, which gives rise to noise like distortions when using OFDM. In the 50Msps case the performance is further limited by the low number of bits.

## V. CONNECTIONS TO OTHER PLATFORMS

The front-end can be connected to other processing platforms that can interface with analog I and Q signals. The digital control of the board can either still be performed by a USRP or to GPIO:s of the new board, where our code for the USRP would be appropriately translated. When connecting to high-speed boards, the band-pass filters (SBP-70) would obviously be removed. Since the RF bandwidth of the Hittite chips is 1.8GHz, sample-rates up to 1.8GHz are useful. Even higher sample-rates could help the shape transmit spectrum but would not increase RF bandwidth further.

Below, we describe how to connect a standard vector signal generator and spectrum analyzer to the boards. In Section VII-A1, we show how to connect a signal generator and oscilloscope to the boards for phase-noise measurements.

## A. VECTOR SIGNAL GENERATOR AND SPECTRUM ANALYZER

A straightforward way to implement an experimental communication link is by means of a vector signal generator as transmitter and a spectrum analyzer as receiver. One problem is that most signal generators and spectrum analyzers have only a single RF port, while the TX and RX boards require both I and Q signals. For smaller transmission bandwidths, this can be solved by using a 90-degree splitter. Here a problem is to find a 90-degree splitter with sufficient bandwidth. Another solution is to simply connect to only one of the inputs of the TX board and one of the outputs of the RX board, as illustrated in Fig. 4. This solution works using well selected center frequencies for the signal generator and vector signal analyzer. Let  $f_{tx-c}$  and  $f_{rx-c}$  be the tuning frequencies of the TX and RX board, respectively; and  $f_g$  and  $f_a$  the center frequencies of the signal generator and spectrum analyzer, respectively. The output signal of TX board will then contain two signal components, one centered around  $f_{tx-c} + f_g$  and the other at  $f_{tx-c} - f_g$ . By selecting the frequencies so that

$$f_{tx-c} + f_g = f_{rx-c} + f_a, \quad (1)$$

but where  $f_{tx-c} \neq f_{rx-c}$ , the received signal can be successfully captured. This has been verified using an Anritsu MG3710A signal generator and a Rohde&Schwarz FX13 vector spectrum analyzer using the settings  $f_g = 620\text{MHz}$ ,  $f_{tx-c} = 59.5\text{GHz}$ ,  $f_{rx-c} = 60.0\text{GHz}$ , and  $f_{rx-c} = 120\text{MHz}$ . A disadvantage of this approach is that half of the transmit power is lost in the image signal.

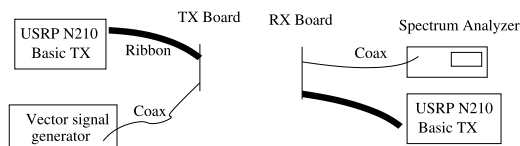


**FIGURE 4.** Vector signal generator + spectrum analyzer setup.

## VI. LINK BUDGET AND LINEARITY RELATED MEASUREMENTS

The results in this section have been obtained using a USRP N210 employing a 25Msps sample rate. The results using 50Msps would be identical since the scaling of the signal sent from the USRP is the same. When using other software defined radio platforms, any reference to the base-band signal level (which we define as the level of the samples input to the UHD driver `uhd::tx_streamer::send` with `complex<int16>` host format) will need to be scaled.

### A. TRANSMIT POWER

Since the transmit chip (HMC6000LP711E) does not provide direct access to the power amplifier output over the air measurements are required. To perform such measurements, the TX board was aligned with a reference horn antenna which

in turn was connected to a spectrum analyzer. The setup is illustrated in Fig. 5. The distance between the TX board and the spectrum analyzer is 0.24m. The reference horn antenna including coaxial cable and adapter loss has an estimated gain of 22.0dBi.

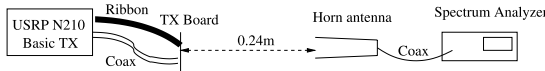


**FIGURE 5.** Setup for EIRP, carrier leakage, image signal and linear gain measurements.

The position of the horn antenna as well as the TX board was adjusted such that the power received by the spectrum analyzer was maximized. The signal input to the TX board was generated using a USRP N210 connected as described in Section IV. The base-band signal was generated using the Matlab function `tx_60GHz.m`, see Section IV-B. The signal generated in base-band was simply a complex sinusoid (cisoid) with varying amplitude. The power received by the spectrum analyzer as a function of amplitude is shown in Fig. 6 for various gain settings. The results for amplitudes of 10000 and higher were not obtained from the spectrum analyzer. Instead, these measurements were done using an RX board (at a distance where linear operation was first verified). The RX board was then used to measure the power at amplitudes of 5000, 10000, 13000, 15000, 20000 and 30000. The relative power increase from amplitude 5000 was then calculated and combined with the spectrum analyzer measurements to complete Fig. 6. The results show saturation with increasing amplitude. The fact that there is saturation also for the smallest gain setting shows that some of the saturation arises already in the base-band or intermediate frequency of the chip. It has been verified that the USRP does not contribute to the saturation.

The maximum power in Fig. 6 is  $-20.6\text{dBm}$ , and is achieved at an amplitude of 30000. Since the free-space omni-directional path-loss is  $55.6\text{dB}$ , the equivalent isotropic radiated power (EIRP) of the TX board is estimated to be  $-20.6 + 55.6 - 22.0 = 13\text{dBm}$ . According to the data-sheet of the chip (HMC6000LP711E), the EIRP should

be  $23.5\text{dBm}$ , thus the result is  $23.5 - 13 = 10.5\text{dB}$  worse. The maximum output power should be achieved when the base-band inputs are at  $-22\text{dBm}$ . In our measurements, the maximum base-band power from the USRP was  $-8.3\text{dBm}$ .

Comparative measurements using another TX board as well as the evaluation board EKIT-HMC6450 have given a similar performance.

## B. RECEIVER SENSITIVITY

The receiver sensitivity of the RX board was estimated by aligning the antenna of a TX board again at a distance of 0.24meters. A cisoid was generated from Matlab with amplitude 5000 and the gain set zero. The signal was captured in Matlab using the `rx_60GHz.m` function; see Section IV-B above. The transmit EIRP is calculated from the results of previous section to be  $-4\text{dBm}$ . The noise bandwidth of the USRP setup using a sampling frequency of 25Msps was estimated to 22.1MHz. Assuming that the receiver antenna achieves its specified  $7.5\text{dBi}$  gain the SNR at the output of a hypothetical receiver with zero dB noise figure can then be calculated using a classical link budget (see [26]) as  $-4.0 - 55.6 + 7.5 + 174 - 10*\log_{10}(22.1\text{e}6) = 48.5\text{dB}$ .

However, in practice an SNR of  $38.5\text{dB}$  was estimated from the data received in Matlab (the noise level was measured prior to switching on the transmitter). This implies that the noise figure of the receiver is  $48.5 - 38.5 = 10\text{dB}$ . The data-sheet of the receiver chip (HMC6000LP711E) states a noise figure of  $7\text{dB}$ , i.e. a difference of  $3\text{dB}$ .

Similar results were achieved using another RX board and using the evaluation board (EKIT-HMC6450). We note that the total link budget is around  $13\text{dB}$  worse than what could be expected from the data-sheets of the chips. However, the bandwidths achieved using the USRP N210 will typically never exceed 25MHz while e.g. the 802.11ad standard uses around 1800MHz. Thus we are still able transmit at same distance as the latest and anticipated future standards.

## C. CARRIER LEAKAGE, IMAGE SIGNAL AND LINEAR GAIN

When performing the measurements in Section VI-A the DC leakage and image signal were also measured for various settings of the analog gain. As described in Section IV, the base-band signals transmitted from the USRP are centered around 70MHz. The rotation of the signal is such that the signal transmitted over air appears at  $f_c - 70\text{MHz}$ , where  $f_c$  is the carrier frequency setting of the TX board. In addition to this signal a CW appears at  $f_c$  and a image signal at  $f_c + 70\text{MHz}$ . The image signal was 30.5 to 47.1dB below the main signal, which is in line with the data-sheet numbers. Fig. 7 shows the strength of the carrier leakage signal (in terms of EIRP) as a function of the analog gain setting. The plot also shows the linear gain at each gain setting. This linear gain  $G$  is

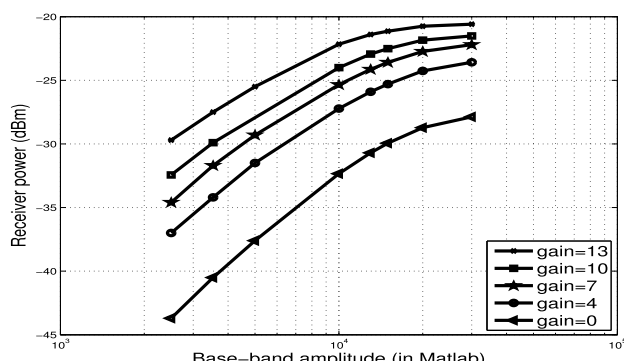


**FIGURE 6.** Power received by the horn antenna.

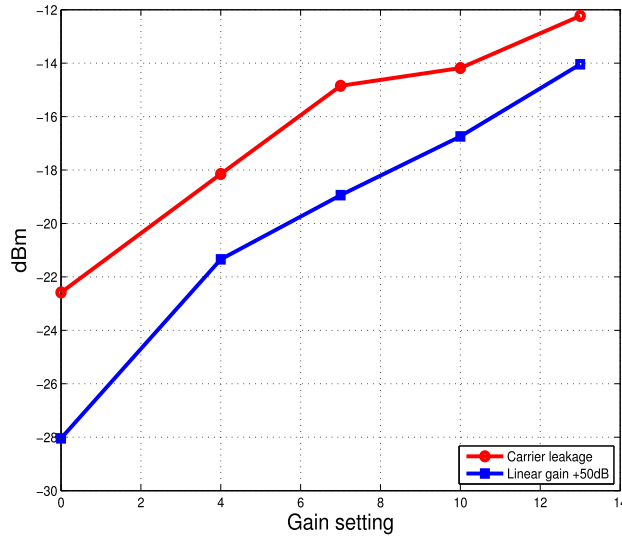


**FIGURE 7.** Carrier leakage and linear gain (in dBm EIRP) as a function of gain setting.

calculated as

$$G = \frac{P(A, g)}{A^2}, \quad (2)$$

where  $P(A, g)$  is the power of the desired signal component,  $A$  is the amplitude of a base-band cisoid signal generated in Matlab (small enough to stay within the linear region), and  $g$  is the gain setting of the TX board. For instance, for a gain setting of 4, we obtain a linear gain of  $G = -21.3 - 50 = -71.3$ dB from the plot. Thus, if a CW of amplitude 1000 (in digital baseband) is transmitted, the output power is  $-71.3 + 20\log_{10}(1000) = -11.3$ dBM (EIRP).

#### D. Intermodulation

In order to facilitate simulations of the impact of non-linear distortion, we have characterized 3rd-order and 5th-order distortions for a number of gain settings. In the measurements, a base-band signal consisting of two tones at frequency offsets  $-2.5$ MHz and  $2.5$ MHz were generated and transmitted using `tx_60GHz.m`, see Section IV-B. The signal was captured

using a spectrum analyzer as in Section VI-A. Fig. 8 shows an example spectrum where the gain is set to 10 and the amplitude of the two tones are 5000. Our aim is to develop a polynomial model of the form

$$y(t) = \beta_1 u(t) + \beta_3 |u(t)|^2 u(t) + \beta_5 |u(t)|^4 u(t), \quad (3)$$

where  $u(t)$  is the base-band complex input signal, and  $\beta_3$  and  $\beta_5$  are nonlinearity constants. These factors are often characterized in the terms of the 3rd and 5th order input intercept points defined as

$$|\beta_3| = |\beta_1|IP3^{-1} \quad (4)$$

and

$$|\beta_5| = |\beta_1|IP5^{-2}, \quad (5)$$

respectively, where IP3 and IP5 correspond to the input power at which the 3rd and 5th order distortion has the same output power as the linear term [27], [28]. Our aim is only to enable assessment of the impact of distortion by simulation. Thus, knowledge of IP3 and IP5 is sufficient. If the goal was the design a pre-distorter a more accurate model would be needed. A common method to estimate IP3 and IP5 is the so-called two-tone measurement where a base-band signal of the form

$$u(t) = A \exp(j(2\pi f_1 t + \phi_1)) + A \exp(j(2\pi f_2 t + \phi_2)) \quad (6)$$

is inserted into the transmitter. Due to the non-linear effects intermodulation products will appear at frequencies  $2f_1 t - f_2$  and  $2f_2 t - f_1$  due to the third order non-linearity (i.e. the second term in (3)) and at  $3f_1 t - 2f_2$  and  $3f_2 t - 2f_1$  due to the fifth order (i.e. the third term in (3)). This is also illustrated by the measurement shown in Fig. 8 where the base-band signal was generated using the function `tx_60GHz.m` with two cisoids of frequency  $+2.5$ MHz and  $-2.5$ MHz (relative to the center frequency) with amplitude and gain set to 5000 and 10, respectively. The IP3 and IP5 can then be estimated as

$$IP3_{dB} = 20 \log(A) + \frac{\Delta P_3}{2} \quad (7)$$

and

$$IP5_{dB} = 20 \log(A) + \frac{\Delta P_5}{4}, \quad (8)$$

respectively, where  $\Delta P_3$  and  $\Delta P_5$  are the power (in dB) of the 3rd and 5th intermodulation components relative to the linear terms, respectively. In our measurements, the power among the the fundamentals and the overtones vary slightly, and we therefore base our estimation on an average. Based on (4,5,7,8) and measurements such as illustrated in Fig. 8 the numerical values in Table 1 are derived. Note that the unit of  $IP3_{dB}$  and  $IP5_{dB}$  refer to the baseband digital representation.

## VII. OPENLY AVAILABLE MEASUREMENTS

### A. PHASE NOISE

In this section we, present time captures of end-to-end phase noise and show how they can be used in hybrid simulation and measurement based investigations.

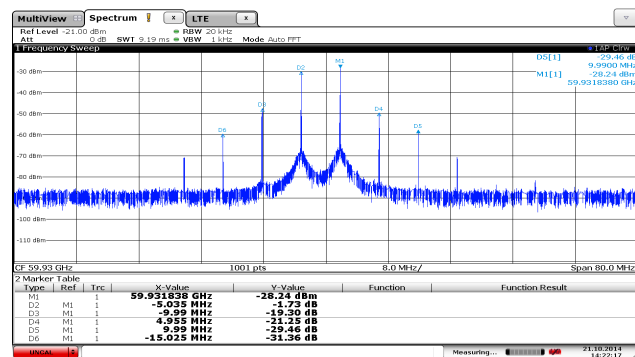


**FIGURE 8.** Spectrum of two-tone test.

**TABLE 1.** Numerical values of 3rd and 5th-order non-linearity parameters.

Gain	IP3 <sub>dB</sub>	IP5 <sub>dB</sub>	$\beta_3/\beta_1$	$\beta_5/\beta_1$
7	84.66	83.20	3.418e-09	2.291e-17
10	80.86	78.33	8.206e-09	2.162e-16
13	78.66	76.93	1.363e-08	4.103e-16

### 1) PHASE NOISE MEASUREMENT SETUP

The setup is illustrated in Fig. 9. The USRP is used to control the digital signals. However, the analog I and Q signals are now generated from a signal generator. In order to create a complex sinusoid, a two-way RF splitter, two attenuators and cables were used. The cable lengths from the splitter are approximately 35cm and 100cm, respectively. The attenuators were used to reduce the impact of impedance mismatches.

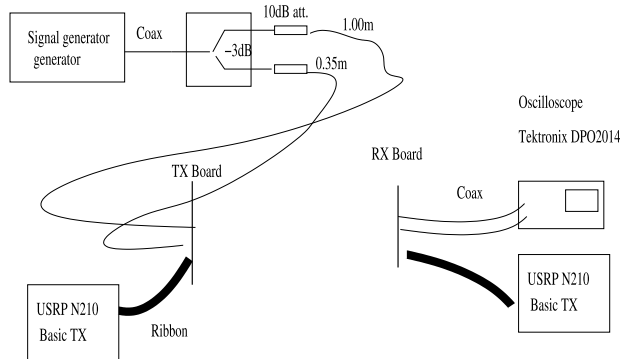


**FIGURE 9.** Phase-noise measurement setup.

By connecting the two signals to an oscilloscope, the frequency at which the two signals are 90degrees offset from each other was found to be 65.67MHz. The phase shift occurs due to delays in the cables.

The outputs of the splitter were connected to the I and Q inputs of the TX board. The I and Q outputs of the RX board were connected to the A and B inputs of a Tektronix DPO2014 sampling Oscilloscope. The data was captured using the instrument control Matlab VISA software (see <http://www.ni.com/visa/>). The oscilloscope allows us to sample almost 100k samples per measurement at a 1GHz sample rate.

### 2) MEASUREMENT ANALYSIS

The phase noise spectrum is estimated by sweeping a sharp 100kHz filter over the received data using different center frequencies. The computations were done in Matlab and the code is available as open source, see Section VIII. The phase noise spectrum obtained from 200 consecutive measurements is shown in Fig. 10. The SNR in the measurements is around 33dB.

Note the the measurement is made from base-band to base-band. The signal sampled by the oscilloscope as a carrier frequency of 65MHz. This makes it possible to use a rather low-cost instrument without stringent timing requirements.

This result in Fig. 10 was also verified by connecting a Rohde&Schwarz FX13 spectrum analyzer to the I connector output of the RX board and performing a phase noise measurement. The result of such a measurement is shown in Fig. 11. By comparing Fig. 10 and Fig. 11 we see that similar results were obtained. The results are also in line with those given in the data-sheet of the chips. There is a peak at around 65MHz in Fig. 11 and in the “No filtering” curve of Fig. 10. This is a harmonic of the received signal. In the signal from the oscilloscope, there are in fact harmonics for every multiple of the input signal frequency. In order to remove this overtone, a filter with cutoff frequency at 64MHz is applied to the data. The result is shown as the “filtered” curve in Fig. 11. In both curves the gain of the I and Q branches was first equalized by applying a scaling factor.

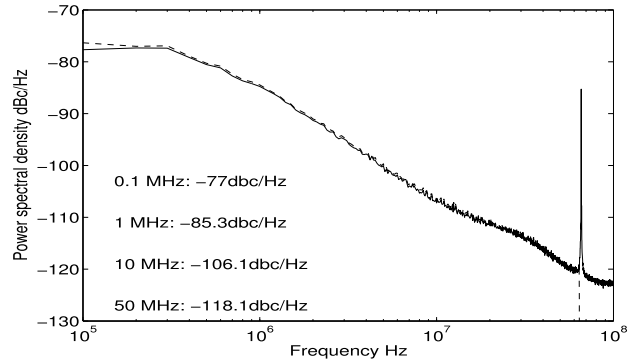


**FIGURE 10.** Estimated phase-noise spectrum from oscilloscope measurements.

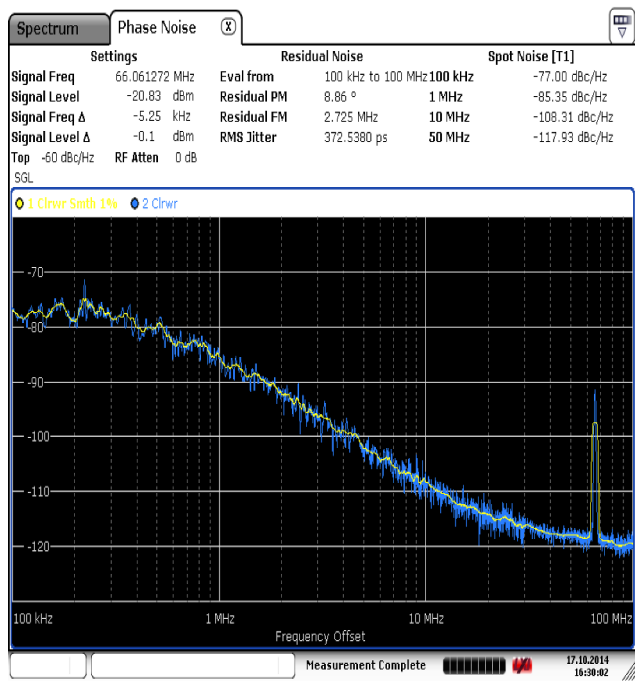


**FIGURE 11.** Estimate of phase-noise spectrum using spectrum analyzer.

A phase noise spectrum does not fully characterize the properties of a signal. Therefore, it is very useful to have measurement traces of phase noise which can be used directly in simulations. Thus in a simulator, a complex valued signal obtained at the receiver  $x(t)$ , is multiplied by a phase noise trace  $p(t)$  so that the phase noise impaired signal becomes

$$\tilde{x}(t) = x(t)p(t). \quad (9)$$

For the benefit of the community, we have made the 200 traces of phase noise available, see Section VIII, where we also provide a function for removing the artifacts not related to the phase-noise phenomena (IQ imbalance and overtones). Note that in equation (9), the assumption is made that all of the phase-noise is introduced at the receiver side, since we are not able to separate the transmitter and receiver phase noise in the measurements. However, this is a common assumption which is valid if the delay-spread of the channel is small compared to phase noise coherence time. An example of how the phase-noise traces can be used is shown in Fig. 12, where the raw bit error rate of an OFDM modulation over a 1GHz bandwidth is shown as a function of the subcarrier spacing on an AWGN channel with ideal channel estimation, synchronization and common phase error correction at a 20dB SNR. The results show that only the smallest investigated DFT size of 100 (which translates into a subcarrier spacing of 10MHz) yields a BER of 1% or lower for all constellation sizes (note that 802.11ad uses a subcarrier spacing of 5MHz). For the largest DFT size of 3200 which corresponds to a subcarrier spacing of 312.5kHz (as in e.g. 802.11ac), only QPSK gives a small bit error rate.

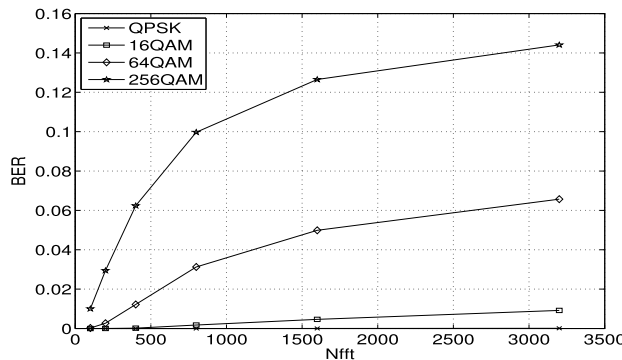


**FIGURE 12.** Raw bit error rate of OFDM signals versus FFT size (sample rate 1GHz).

So far we have discussed the use of the phase-noise measurements for simulation of SISO systems. For MIMO systems, we may consider two different cases. In the first case, “common LO”, the multiple transmitter chains of the transmitter uses the same LO and likewise at the receiver. In the second case, “individual LO”, each transmitter and receiver branch has its own LO. In the “common LO” case, the received signal is simulated by simply multiplying the

received signal by a phase-noise trace as

$$\tilde{\mathbf{x}}(t) = \mathbf{x}(t)p(t) \quad (10)$$

where  $\mathbf{x}(t)$  is the phase-noise free received vector of signals and  $\tilde{\mathbf{x}}(t)$  is the impaired vector of signals and  $p(t)$  is a single phase-noise trace. In the “individual LO” case, we propose the following: The signal received on antenna  $j$  is given by

$$\tilde{x}_j(t) = \sum_{n=1}^{M_{\text{TX}}} p_{j,n}(t)x_{j,n}(t), j = 1, \dots, M_{\text{RX}}, \quad (11)$$

where  $x_{j,n}(t)$  is the phase-noise free received signal contribution from transmitter antenna  $n$  and  $p_{j,n}(t)$  the corresponding phase-noise. We propose that all  $M_{\text{RX}} \times M_{\text{TX}}$  phase noise signals are taken from different measured phase noise traces. This is a somewhat pessimistic assumption since the phase noises  $p_{j_1,n_1}(t)$  and  $p_{j_2,n_2}(t)$ , will in fact not be independent when  $j_1 = j_2$  or  $n_1 = n_2$ .

Another aspect of signal phases which is important for beamforming systems is the long-term phase stability between branches connected to the same CLK board. The phases change arbitrarily each time the boards are re-started, due to the random startup state of the PLLs. However, between the re-starts, the phase offset are stable. In order to quantify the long-term stability, a measurement was performed were one TX board was transmitting and two RX boards where receiving. Fifty frames where captured, each having 10000 samples (0.4ms in duration at 25Msps). The local mean phase offset between the two RX boards was estimated for each frame. The standard deviation of the local mean offsets were estimated to 7.8 degrees, and the difference between the maximum and minimum phase offset was 32 degrees. The time between the frames was 5.6 seconds and thus the total duration was 4.7minutes. A beamforming system must have a procedure to calibrate the average phase offsets between the branches.

## B. MIMO MEASUREMENTS (2 × 2)

MIMO measurements ( $2 \times 2$ ) were performed in the same location as the companion video demonstration. Two TX boards are mounted so that one has horizontal and the other vertical polarization. The same is done at the receiver. This creates a channel matrix where the off-diagonal elements are small. The receiver board is moved from close to the transmitter to just outside the door of the office room, as illustrated in Fig. 13. The maximum distance is about three meters and the measurement ends in a non line-of-sight position. This is done ten times. Each time, the receivers capture around ten files, each of which contains 30000 samples. In the first five measurements, the receiver and transmitter board are held in a horizontal position, while in the other five measurements the receiver board is tilted some 45 degrees in order to create a non-diagonal channel matrix.

The transmission was done so that so that a synchronization sequence is transmitted first, then an OFDM burst is

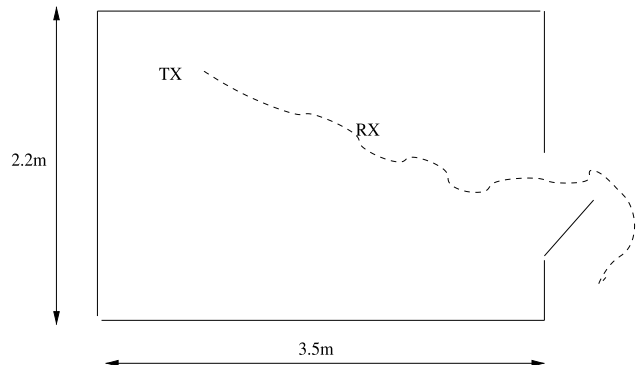


**FIGURE 13.** The dotted line illustrates the measurement trajectory during the  $2 \times 2$  MIMO measurements.

transmitted where both TX antennas sends a different stream of symbols. Then two burst are sent where first only antenna number one is active and then antenna number two. Since no pre-coding is applied at the transmitter, we use these two sequences to evaluate the would-be performance without cross-channel interference.

All the measurements and post-processing script have been made publicly available, see Section VIII. The bit error rate has been estimated from the collected data.

The performance is shown in Fig. 14 and Fig. 15. Fig. 14 shows histograms of the raw bit error rate per

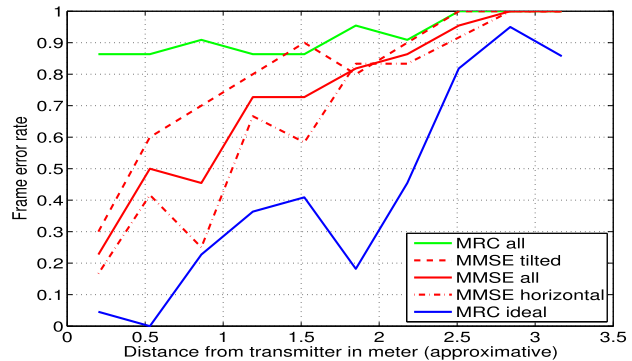


**FIGURE 15.** Frame error rate as a function of the distance from the transmitter.

frame for QPSK modulation using all the 220 transmitted frames. The upper plot corresponds to maximum ratio combining (MRC) in the receiver, the second plot to an MMSE receiver (for maximum ratio combining and MMSE see [29]), and the third to the interference free case (where naturally a maximum ratio combining is used). The results clearly show the improvement of MMSE over MRC and a further improvement when there is no cross-channel interference. Fig. 15 shows the frame error rate (FER) as a function of the transmitter to receiver distance (a frame is assumed to be in error if one or more bits are in error). This figure shows that the cross channel interference is responsible for a good portion of the errors - and the worse conditions when the receiver is tilted. The most distant measurements ( $>2.8$ meters) are in NLoS, and no signal is detected there.

It is possible that the performance in the interference free case could also be obtained in the case with interference. Due to hardware impairments, the stronger signal carries with it a distortion noise which hides the weaker signal. However, if power control is employed, it may be possible to lower the stronger signal and thus reduce its drowning effect. Such techniques can be tested by weighting the signals from each transmitter and then adding them before processing. Each measurement file also contains at least one repetition of all the transmitted signals (by stepping forward 9000 samples) which allows feedback delay effects to be accounted for in the simulation. Other dirty-RF compensation techniques can also be evaluated using the data.

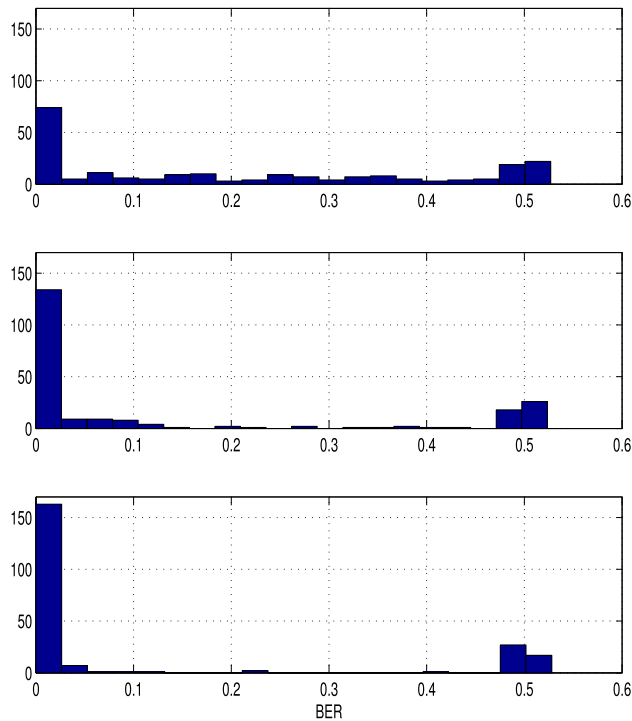


**FIGURE 14.** Raw BER of QPSK. Upper: maximum ratio combining; middle: MMSE; lower: Interference free maximum ratio combining.

## VIII. OPEN RESOURCES

The software, the measurements and the hardware design files are available in the `open_source_60GHz.tar.gz` archive which is supplied as a supplemental file for this article. The software is located in the directory with that name. A list of files and instructions on how to compile is given in the README file in the directory. All the files used to control the boards, the SISO and  $2 \times 2$  MIMO applications, and the scripts used to generate the results from the phase-noise and MIMO measurements are provided.

The phase noise measurements, the  $2 \times 2$  MIMO measurements and the hardware design files are available in the directories `phase_noise_measurements`, `MIMO_signals` and `Hardware_design`, respectively. How to use the phase-noise and  $2 \times 2$  MIMO measurements is evident from the Matlab/octave files in the software directory. The hardware design folder contains two versions of the board design with associated Gerber files, drill files, schematics and bill of material; see the `README` file for more information.

## IX. CONCLUSION

We have introduced an open source platform aimed at mm-wave wireless experimentation in the 60GHz band. The purpose is to allow a wider range of research groups to do testbed implementations in the 60GHz band than what is presently possible. We provide the hardware design, software and measurements. The measurements allow hybrid simulation and measurements studies with hardware impairments specific for the mm-wave application even without the hardware. In the paper, we have also demonstrated MIMO spatial multiplexing using the platform.

The platform can be used for proof of concept demonstration for e.g. ultra-dense networks. Here one may need to extrapolate the performance that would be obtained with a higher output power, higher antenna gain and wider bandwidth. Other uses include using the phase-noise measurements in link-level simulations. The amplifier non-linearities can also be used in link-level simulations. For instance, by using high-speed DAC and ADC boards and measuring the impact of distortions. Other uses include the investigation of relaying schemes and positioning. Finally, as mentioned in Section III, by mounting several Hittite chips on a PCB in a irregular fashion, it may be possible to realize narrow beams without excessive side lobe levels. It should at least be possible to achieve significant array gains.

## REFERENCES

- [1] T. S. Rappaport *et al.*, "Millimeter wave mobile communications for 5G cellular: It will work!" *IEEE Access*, vol. 1, pp. 335–349, 2013.
- [2] T. S. Rappaport, J. N. Murdock, and F. Gutierrez, "State of the art in 60-GHz integrated circuits and systems for wireless communications," *Proc. IEEE*, vol. 99, no. 8, pp. 1390–1436, Aug. 2011.
- [3] H. Yang, P. F. M. Smulders, and M. H. A. J. Herben, "Indoor channel measurements and analysis in the frequency bands 2 GHz and 60 GHz," in *Proc. IEEE 16th Int. Symp. Personal, Indoor Mobile Radio Commun. (PIMRC)*, vol. 1, Sep. 2005, pp. 579–583.
- [4] H. Xu, V. Kukshya, and T. S. Rappaport, "Spatial and temporal characteristics of 60-GHz indoor channels," *IEEE J. Sel. Areas Commun.*, vol. 20, no. 3, pp. 620–630, Apr. 2002.
- [5] T. Schenk, *RF Imperfections in High-Rate Wireless Systems: Impact and Digital Compensation*. Berlin, Germany: Springer-Verlag, 2008.
- [6] A. Osseiran *et al.*, "Scenarios for 5G mobile and wireless communications: The vision of the METIS project," *IEEE Commun. Mag.*, vol. 52, no. 5, pp. 26–35, May 2014.
- [7] R. Baldemair *et al.*, "Ultra-dense networks in millimeter-wave frequencies," *IEEE Commun. Mag.*, vol. 53, no. 1, pp. 202–208, Jan. 2015.
- [8] A. L. Swindlehurst, E. Ayanoglu, P. Heydari, and F. Capolino, "Millimeter-wave massive MIMO: The next wireless revolution?" *IEEE Commun. Mag.*, vol. 52, no. 9, pp. 56–62, Sep. 2014.
- [9] T. Baykas *et al.*, "IEEE 802.15.3c: The first IEEE wireless standard for data rates over 1 Gb/s," *IEEE Commun. Mag.*, vol. 49, no. 7, pp. 114–121, Jul. 2011.
- [10] T. Nitsche, C. Cordeiro, A. B. Flores, E. W. Knightly, E. Perahia, and J. C. Widmer, "IEEE 802.11ad: Directional 60 GHz communication for multi-gigabit-per-second Wi-Fi [Invited Paper]," *IEEE Commun. Mag.*, vol. 52, no. 12, pp. 132–141, Dec. 2014.
- [11] A. Alkhateeb, O. El Ayach, G. Leus, and R. W. Heath, "Hybrid precoding for millimeter wave cellular systems with partial channel knowledge," in *Proc. Inf. Theory Appl. Workshop (ITA)*, Feb. 2013, pp. 1–5.
- [12] T. Nitsche, A. B. Flores, E. W. Knightly, and J. Widmer, "Steering with eyes closed: mm-wave beam steering without in-band measurement," in *Proc. 34th IEEE Int. Conf. Comput. Commun.*, Apr. 2015.
- [13] S. Sun, T. S. Rappaport, R. W. Heath, A. Nix, and S. Rangan, "MIMO for millimeter-wave wireless communications: Beamforming, spatial multiplexing, or both?" *IEEE Commun. Mag.*, vol. 52, no. 12, pp. 110–121, Dec. 2014.
- [14] X. Tie, K. Ramachandran, and R. Mahindra, "On 60 GHz wireless link performance in indoor environments," in *Passive and Active Measurement*, N. Taft and F. Ricciato, Eds. Berlin, Germany: Springer-Verlag, Mar. 2012, pp. 147–157.
- [15] J. Beas, G. Castanon, I. Aldaya, A. Aragon-Zavala, and G. Campuzano, "Millimeter-wave frequency radio over fiber systems: A survey," *IEEE Commun. Surveys Tuts.*, vol. 15, no. 4, pp. 1593–1619, 2013.
- [16] Y. Zhu *et al.*, "Demystifying 60 GHz outdoor picocells," in *Proc. 20th ACM Int. Conf. Mobile Comput. Netw.*, Mar. 2014, pp. 5–16.
- [17] W. Keusgen, A. Kortke, M. Peter, and R. Weiler, "A highly flexible digital radio testbed and 60 GHz application examples," in *Proc. Eur. Microw. Conf. (EuMC)*, Oct. 2013, pp. 740–743.
- [18] A. Demir, A. Mehrotra, and J. Roychowdhury, "Phase noise in oscillators: A unifying theory and numerical methods for characterization," *IEEE Trans. Circuits Syst. I, Fundam. Theory Appl.*, vol. 47, no. 5, pp. 655–674, May 2000.
- [19] A. Mehrotra, "Noise analysis of phase-locked loops," *IEEE Trans. Circuits Syst. I, Fundam. Theory Appl.*, vol. 49, no. 9, pp. 1309–1316, Sep. 2002.
- [20] M. A. Hossain, H. Lin, and K. Yamashita, "Low-complexity blind phase noise compensation in OFDM systems," in *Proc. Int. Conf. Elect. Eng. Inf. Commun. Technol. (ICEEICT)*, Apr. 2014, pp. 1–4.
- [21] H. Mehrpoyan, A. A. Nasir, S. D. Blostein, T. Eriksson, G. K. Karagiannidis, and T. Svensson, "Joint estimation of channel and oscillator phase noise in MIMO systems," *IEEE Trans. Signal Process.*, vol. 60, no. 9, pp. 4790–4807, Sep. 2012.
- [22] E. Bjornson, J. Hoydis, M. Kountouris, and M. Debbah, "Massive MIMO systems with non-ideal hardware: Energy efficiency, estimation, and capacity limits," *IEEE Trans. Inf. Theory*, vol. 60, no. 11, pp. 7112–7139, Nov. 2014.
- [23] W. A. van Cappellen, S. J. Wijnholds, and J. D. Bregman, "Sparse antenna array configurations in large aperture synthesis radio telescopes," in *Proc. 3rd Eur. Radar Conf. (EuRAD)*, Sep. 2006, pp. 76–79.
- [24] S. K. Reynolds *et al.*, "A silicon 60-GHz receiver and transmitter chipset for broadband communications," *IEEE J. Solid-State Circuits*, vol. 41, no. 12, pp. 2820–2831, Dec. 2006.
- [25] Y. P. Zhang, M. Sun, K. M. Chua, L. L. Wai, D. Liu, and B. P. Gaucher, "Antenna-in-package in LTCC for 60-GHz radio," in *Proc. Int. Workshop Antenna Technol., Small Smart Antennas Metamater. Appl. (IWAT)*, Mar. 2007, pp. 279–282.
- [26] L. Ahlin and J. Zander, *Principles of Wireless Communications*, 2nd ed. Studentlitteratur, 1998.
- [27] W. Sansen, "Distortion in elementary transistor circuits," *IEEE Trans. Circuits Syst. II, Analog Digit. Signal Process.*, vol. 46, no. 3, pp. 315–325, Mar. 1999.
- [28] K. Chan. (Mar. 2013). "The IP3 specification—Demystified," Maxim Integr., San Jose, CA, USA, Tech. Rep. 5429. [Online]. Available: <http://www.maximintegrated.com/en/app-notes/index.mvp/id/5429>
- [29] D. Tse and P. Viswanath, *Fundamentals of Wireless Communication*. Cambridge, U.K.: Cambridge Univ. Press, 2005.



**PER ZETTERBERG** received the M.S. degree from Luleå University, Luleå, Sweden, in 1992, and the Ph.D. degree in electrical engineering from the KTH Royal Institute of Technology, Stockholm, Sweden, in 1997. He then joined Radio Design AB, where he was involved in smart antenna research and implementation. Since 2002, he has been with the Signal Processing Laboratory, ACCESS Linnaeus Center, KTH Royal Institute of Technology, working full-time in wireless testbeds and radio propagation. He has been instrumental in some of the earliest experimentation with cellular switched-beam systems, multiuser multiple-input and multiple-output, multicell propagation correlations, high-order sectorization, cooperative relaying, coordinated multipoint, and interference alignment. He is or has been involved in the EU projects, such as TSUNAMI II, NEWCOM, SATURN, ACE, WINNER, WINNER II, COOPCOM, and HIATUS. He has authored some 70 journal and conference papers, and has an h-index of 16 in a Google Scholar.



**RAMIN FARDI** received the M.Sc. degree from the KTH Royal Institute of Technology, in 1994. From 1992 to 1995, he was with Ericsson Radio Access, where he was involved in Very High Speed Integrated Circuit Hardware Description Language logic synthesis for base-station modems. He then joined Radio Design AB, a start-up company, where he was involved in software defined radio, radio platform design, and feedforward linearized amplifiers. From 1999 to 2000, he was employed by SwitchCore AB, where he was involved in the physical layer hardware of gigabit Ethernet switches. Since 2000, he has been with Bluewave Microsystems AB, where he has worked with projects in cellular base-station power amplifiers, analytical measurement instruments, spectroscopy, wireless sensors, and industrial control.

• • •